International Journal of Non-Linear Mechanics 45 (2010) 42–55

Contents lists available at ScienceDirect

International Journal of Non-Linear Mechanics

journal homepage: www.elsevier.com/locate/nlm

Identifying invariant manifold using phase space warping and stochastic interrogation

Joe Kuehl [a,b], David Chelidze [a,*]

[a] Nonlinear Dynamics Laboratory, Department of Mechanical , Industrial and Systems Engineering, University of Rhode Island, Kingston, RI 02881, USA
[b] Graduate School of Oceanography, University of Rhode Island, Kingston, RI 02881, USA

ARTICLE INFO

Article history:
Received 14 October 2008
Received in revised form
14 July 2009
Accepted 5 September 2009

Keywords:
Lagrangian coherent structures
Invariant manifolds
Phase space warping
Stochastic interrogation
Finite-time Lyapunov exponent

ABSTRACT

Advances in the generalization of invariant manifolds to finite time, experimental (or observational) flows have stimulated many recent developments in the approximation of invariant manifolds and Lagrangian coherent structures. This paper explores the identification of invariant manifold like structures in experimental settings, where knowledge of a flow field is absent, but phase space trajectories can be experimentally measured. Several existing methods for the approximation of these structures modified for application when only unstructured trajectory data is available. We find the recently proposed method, based on the concept of phase space warping, to outperform other methods as data becomes limited and show it to extend the finite-time Lyapunov exponent method. This finding is based on a comparison of methods for various data quantities and in the presence of both measurement and dynamic noise.

1. Introduction

In dissipative dynamical systems, such as structural or mechanical vibrations problems, basins of attraction are of great importance. Once identified, these basin provide information about admissible future states of the system (by definition), may be used to predict transitions to chaos [10,2] through heteroclinic or homoclinic tangles, increase our overall understanding of the system and have potential for control scheme design in machine processes. These basins are often delineated by the stable invariant manifolds of the system's phase space. Invariant manifolds are also a useful tool for estimating chaotic mixing [1,3], and provide a means to understand the underlying structure of complex flows [4]. This work is concerned with the largely unexplored case of invariant manifold detection from experimentally obtained phase space trajectories.

When applying invariant manifold techniques to experimental vibrations data several issues must be considered. First, these are experimental records that provide *finite time* snapshots of a system. The stable invariant manifold is defined as $\{\vec{x}_0|\lim_{T\to\infty}\vec{x}\to\vec{x}^*\}$, the set of initial states which approach a hyperbolic trajectory with "saddle like behavior", $\vec{x}^*$, under forward time iteration [5], while the unstable manifold is defined as $\{\vec{x}_0|\lim_{T\to-\infty}\vec{x}\to\vec{x}^*\}$. The infinite time limit present in these definitions is not a trivial problem to overcome. Indeed, there is no agreed-upon generalization of invariant manifolds to finite-time flows. Second, only a finite amount of trajectory data is available. Most existing manifold detection methods rely on the ability to conveniently place numerical trajectories where desired. For the present case, this is only possible if the trajectory data is used to approximate a flow field, which is then used to estimate hypothetical trajectories. Finally, noise is present in all experimental data, and must be considered. We investigate the effects of both additive measurement noise, as well as dynamic noise.

Recently much work has been focused on the finite-time generalization of invariant manifolds with two schools of thought dominating the field. The first is based on a generalization of the infinite-time invariant manifold definition. It seeks to identify finite-time hyperbolic trajectories with "saddle-like" behavior, usually by maximizing some measure of hyperbolicity following a trajectory. Several different names have been associated with these special trajectories, *uniformly hyperbolic trajectories* (UHT) [24], *distinguished trajectories* (DT) [23], and *distinguished hyperbolic trajectory* (DHT) [6]. Once identified, one attempts to "grow" manifolds off these trajectory by initializing secondary trajectories along their stable and unstable eigenspaces. Since the secondary trajectories lie (approximately) on the stable (unstable) manifold, they trace out the manifolds location under backwards (forward) time iteration.

While these methods provide a definition for finite-time structures which is consistent with invariant manifolds in the infinite-time limit, its application to experimental data is limited.

* Corresponding author. Tel.: +1 401 874 2356; fax: +1 401 874 2355.
E-mail addresses: jkuehl@gso.uri.edu (J. Kuehl), chelidze@egr.uri.edu (D. Chelidze).
URL: http://mcise.uri.edu/chelidze/ (D. Chelidze).

0020-7462/$ - see front matter © 2009 Elsevier Ltd. All rights reserved.
doi:10.1016/j.ijnonlinmec.2009.09.001

To apply these methods, the hyperbolic trajectory must first be located. In the present case, flow data can only be reproduced in regions where trajectories are present. As these special hyperbolic trajectories are unstable structures, their locations will be sparsely populated and the flow field will not be well reconstructed around them. Even if the hyperbolic trajectory's location is initially populated, it will not remain so long enough for the identification algorithms to converge. If the hyperbolic trajectory could be located, and its stable and unstable eigenspaces could be identified, secondary trajectories must still be tracked to trace out the manifolds. Other than the accuracy needed to trace the manifold, there is an additional obstacle; the manifolds are traced in their unstable form. This requires running time backwards to trace the stable manifold, thus starting from the end of our data record. It will be shown that we can begin our data record with a randomly populated space, but as the system evolves, trajectories will converge to any attractors present. When attempting to run time backwards, we can only track trajectories initialized in the region of the attractors, not the region around an unstable hyperbolic trajectory. These limitations represent significant obstacles to applying the "growing" methods to general aperiodic flows, but do not prohibit their application. If the flow is periodic, for instance, it may be possible to obtain a high enough resolution stroboscopic Poincaré map to accurately iterate trajectories. However, due to the discussed limitations, we will focus our investigation on the second school of thought.

The second school of thought seeks to identify structures in the flow which posses properties normally associated with invariant manifolds. We are interested in invariant manifolds because they have certain properties; thus, despite clear finite-time definitions, we aim to identify structures in the flow with those same properties (delineate basins of attraction, organize the flow, etc.). As this is the case, we use our knowledge/intuition of invariant manifolds to build detection schemes which identify invariant manifold like behavior. The most popular of these methods seeks to identify ridges in stretching fields of the flow by calculating the *finite-time Lyapunov exponent* (FTLE). These structures have been named *Lagrangian coherent structures* (LCS) and have been shown to exhibit properties similar to invariant manifolds [7]. We favor this second school of thought, which is a more practical approach, as will be demonstrated by the methods considered, for application oriented studies. The lack of flow data will be addressed by modifying several existing methods for use when only trajectory data is available as well as attempting to reconstruct flow data from the available trajectory data. Each of the proposed methods will be tested for measurement and dynamic noise sensitivity, as well as data quantity limitations.

We propose five methods which are tested on simulated experimental data of a vibrating cantilever beam buckled by a non-linear potential at the free tip (i.e., Moon's beam [8]). This is accomplished by numerically applying the method of *stochastic interrogation* [9,10] to the damped, harmonically driven two-well Duffing equation, which was shown to be a good one-degree-of-freedom approximation for the stiffened beam apparatus described in Ref. [9]. The five considered methods are: (1) closest approach, which is an approximation to the growing methods; (2) cloud deformation, which is an approximation to stretching based techniques; (3) particle divergence [11], which is a simple theory motivated by the geometric interpretation of invariant manifolds; (4, 5) velocity field reconstruction, which is explored in conjunction with both the FTLE method and a new method based on the concept of *phase space warping* (PSW) [12]. It is our hope that the basic introduction and justification of the PSW method given in this work will stimulate a further and more rigorous treatment of the method. Note unless otherwise stated, all figures are typical phase space representations with position on the horizontal axis and velocity on the vertical. Each figure is plotted after considering data equivalent to four forcing periods of integration on a 0.01×0.01 mesh grid.

2. Simulated model and reference data

A numerically generated data set is considered, so that each method may be tested against a reference manifold calculation. The numerical data is computed in such a way that it mimics experimental data obtained by the method of Stochastic Interrogation. Stochastic Interrogation is a method which randomly populates the phase space of a periodically forced system by switching between modes of stochastic and periodic forcing. Consider a periodically forced system. From a given initial condition, the system is allowed to evolve in time for T_p periods while data is being collected. The forcing is then replaced by a stochastic forcing which is allowed to act for T_s periods. At the end of the stochastic forcing interval, the system will find itself in a new (random) initial condition. At this point, periodic forcing is once again applied and the system is allowed to evolve from the new initial condition while data is being collected. In this way, the system's phase space may be randomly populated. This method relies on the periodicity of the forcing. Each data collection interval starts at the same forcing phase, but with a new initial condition.

The damped, harmonically driven, two-well Duffing equation integrated with a fourth order Runge–Kutta scheme, is chosen for investigation:

$$\ddot{x}+\mu\dot{x}-\alpha x+\beta x^3=f\sin\omega t, \tag{1}$$

with $\mu=0.044$, $\alpha=0.7627$, $\beta=0.5536$, $\omega=2\pi/5$, and $f=0.1$. Parameters α and β are taken from Ref. [9], which represent their experimental apparatus well. μ is chosen small to avoid rapid convergence to the systems fixed points (half the value used in Ref. [9]). It should be noted that for the parameters chosen here, the system is chaotic and the manifold will have a fractal structure shown in Fig. 1. If the system is allowed to evolve long enough that each trajectory has settled to a fixed point, the basins of attraction can be easily identified by labeling initial states based on which fixed point the trajectory settles to. The boundary between these basins of attraction is the stable manifold. However, this would require a very long time, both experimentally and numerically. One strength of the methods considered here, is their success with

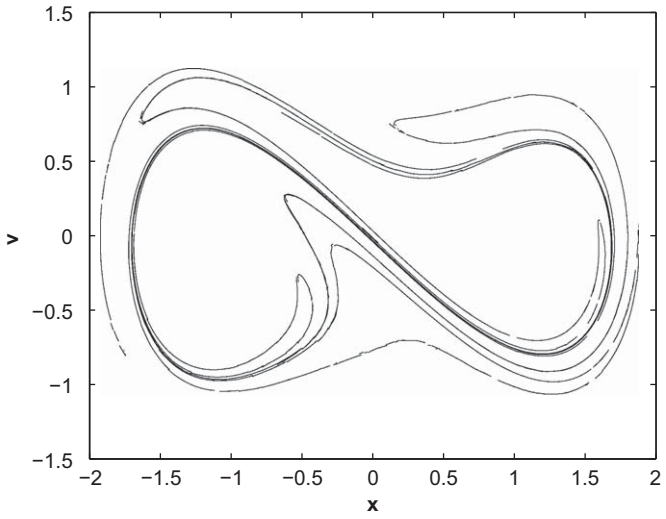

Fig. 1. Reference manifold calculated by the method of "growing" (discussed in Section 3.1), using Eq. (1), after four periods of evolution.

short-time data in which the trajectories are far from converging to the fixed points of the system. Indeed, with $\mu = 0$ (conservative system) these methods are still capable of identifying invariant manifold like behavior.

Stochastic forcing is achieved by generating a sequence of random numbers that then replaces the right hand side of Eq. (1) as the forcing term during stochastic forcing intervals. The system was integrated for $T_s = 25$ periods stochastically forced, then allowed to evolve for $T_p = 10$ periods of periodic forcing. Only four forcing periods of evolution are used for manifold detection, as this provides sufficient detail to validate each method, though a longer data collection interval may be used to obtain more manifold structure. This sequence was repeated until the phase space was suitably populated. Two populations are considered, 2×10^4 and 5×10^3 trajectories, which represent abundant and sparse data sets, respectively. For some detection schemes the system must be reduced to a stroboscopic Poincaré map, φ, by down-sampling each trajectory once per period at constant phase ϕ. Under φ the saddle point and its manifolds become fixed. The evolution of the manifolds may be explored by varying ϕ.

Both measurement noise and dynamic noise are investigated at the 15% level, defined as the ratio of noise amplitude to forcing amplitude. Measurement noise is simulated by addition of randomly generated numbers to the trajectory data. Dynamic noise is incorporated by addition of randomly generated numbers to the amplitude of the forcing term in Eq. (1) during the numerical integration. In general, all experimental applications will be simultaneously subject to both types of noise. It is, however, insightful to consider their effects separately. The floor function is applied to each random number for interpolation purposes during numerical integration.

3. Methods for invariant manifold identification[1]

3.1. Closest approach

The closest approach method is an attempt to adapt the "growing" (or "straddling") method for trajectory only data. The "growing" method uses the fact that any trajectory located on the invariant manifold remains on the invariant manifold, hence "invariant". With knowledge of a DHT, secondary trajectories are initialized along its stable (unstable) eigenspace and tracked in backward (forward) time. The invariant manifolds near to the DHT are tangent to the linearized eigenspaces, so that the eigenspaces, close enough to the DHT, are a good approximation to the invariant manifolds. Thus, one is able to populate a small portion of the manifold with secondary trajectories. These trajectories then trace out the entire manifolds location. This method was used to calculate a reference manifold directly from Eq. (1) (as shown in Fig. 1). The saddle point was located by initializing a grid of trajectories over its expected location. The grid is stretched along the unstable direction and compressed along the stable direction. This process was repeated until the saddle point along with its stable and unstable eigenspaces were suitable identified. Far more sophisticated variations of the "growing" method are used for more accurate calculations [13], but the simple version will suffice here.

For trajectory only data, one cannot integrate secondary trajectories, unless the flow is reconstructed. However, for the current data set, when reduced to a Poincaré map, it is possible to approximate the location of a saddle point. This may be accomplished by physical arguments, inspection of the data set itself, or by one of the methods provided later. A saddle is an unstable structure, so the only way a trajectory may come close to it, is for the trajectory to be located near to the stable manifold. Therefore, with knowledge of the saddle location, we calculate the distance of closest approach, R, between each trajectory and the saddle location. Those trajectories which minimize R (or maximize R^{-1}) will approximate the location of the stable manifold (calculation results for our data are shown in Fig. 2). This method works well for stationary and periodic systems (reduced to a Poincaré map), in which the saddle is fixed. For aperiodic systems, a DHT would need to be identified and tracked, before distance of closest approach may be calculated. This is likely to be a prohibitive limitation of this simple method.

3.2. Stretching based scheme

Stretching based schemes are motivated by the geometric interpretation of invariant manifolds. Consider two trajectories which lie on either side of the stable invariant manifold. As these trajectories evolve forward in time, they will rapidly diverge from one another as they approach the saddle point. This represents significant stretching of the phase space, and led Bowman [11] to propose a simple yet powerful method for identification of invariant manifolds, where the divergence between pairs of trajectories is calculated. If the trajectories diverge rapidly, a stable manifold may lie somewhere between them. When the flow field is given, a grid of particles may be initialized and divergence between adjacent pairs may be calculated. One then looks at the divergence field for manifold like structures. For trajectory only data, we cannot systematically consider nearest neighbor trajectories. Since the orientation of pairs is not structured, there is no guarantee pairs will be oriented such that they straddle a manifold. Instead, we locate a group of four nearest neighbors at a given time. Then calculate the divergence between each pair in the group. The pair with maximal divergence in the group is used to identify stretching for that region of phase space as shown in Fig. 3.

A caution to considering trajectory pair divergence is provided by Winkler [14]. Attention must be paid to the integration time. For long times, the pair may become uncorrelated due to diffusion, viscus effects, or error accumulation, and no longer represent a deterministic stretching. Also, for closed basins and chaotic motion, trajectories which initially diverge may find themselves once again in close proximity after a long enough time. To alleviate these effects renormalization may be incorporated. This renormalization results in removing the distance dependence of stretching and only considers local stretching around the trajectory of interest. A popular method for determining this local stretching is the Lyapunov exponent. Wolf et al. [15] provides a method for determining the first few non-negative Lyapunov exponents from trajectory data. In general, Lyapunov exponents provide information on predictability of the system and are useful for approximating the dimension of an attractor [21].

The connection between FTLE and stretching is nicely illustrated in the following example, which is used to motivate the definition of FTLE. Consider the map $\vec{\varphi}(\vec{x}_n) = \vec{x}_{n+1}$. Under the action of $\vec{\varphi}$, the separation between two nearby trajectories, $\Delta\vec{x}_n$, will evolve as

$$\Delta\vec{x}_{n+1} = \vec{\varphi}(\vec{x}_n) - \vec{\varphi}(\vec{x}_n + \Delta\vec{x}_n), \tag{2}$$

and the second term may be Taylor expanded about $\vec{x}_n$:

$$\Delta\vec{x}_{n+1} = \vec{\varphi}(\vec{x}_n) - [\vec{\varphi}(\vec{x}_n) + D\vec{\varphi}(\vec{x}_n)\Delta\vec{x}_n + O(\|\Delta\vec{x}_n\|^2)], \tag{3}$$

where D is a differential operator with respect to $\vec{x}_n$. For small $\Delta\vec{x}_n$, higher order terms may be ignored, and defining $F \equiv D\vec{\varphi}(\vec{x}_n)$,

[1] Basic components of the MATLAB codes used in the simulations can be found here: http://www.mce.uri.edu/chelidze/nld/software/.

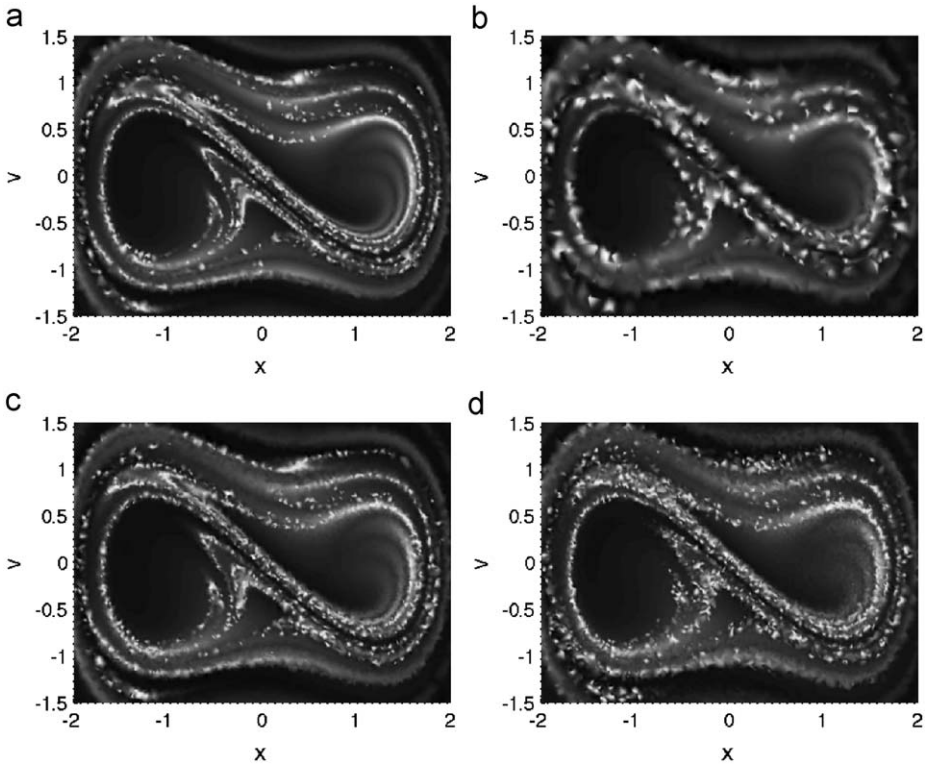

Fig. 2. Manifold approximated by the closest approach method. Intensity field of R^{-1} is shown with light areas corresponding to closest approaches: (a) abundant data (2×10^4 trajectories), (b) sparse data (5×10^3 trajectories), (c) 15% measurement noise (2×10^4 trajectories), and (d) 15% dynamic noise (2×10^4 trajectories).

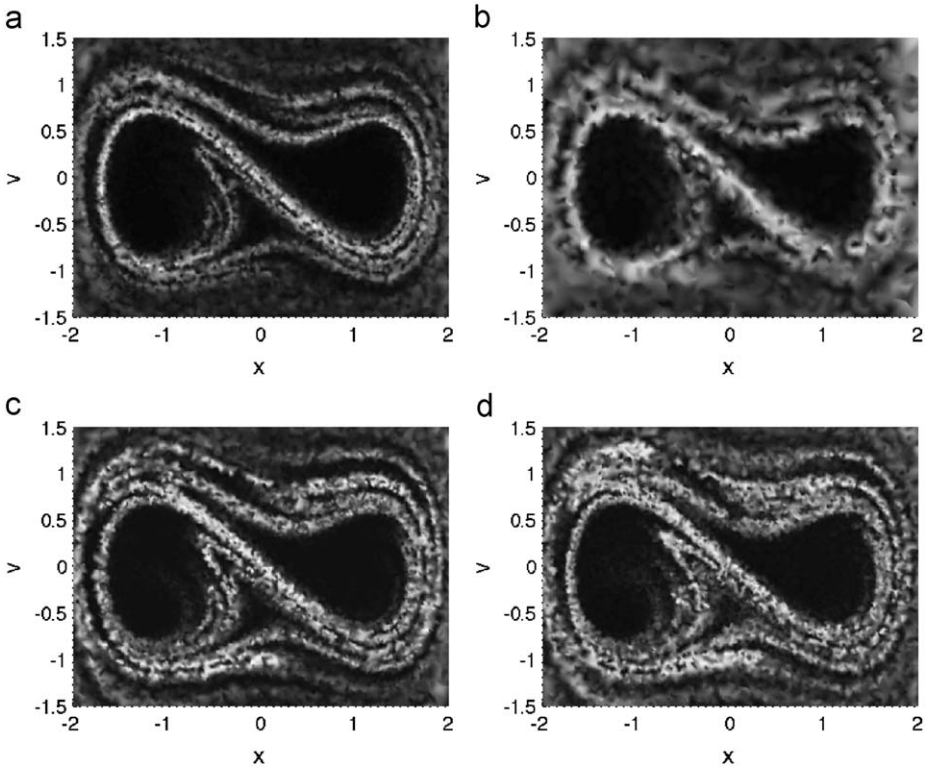

Fig. 3. Manifold approximated by the particle divergence method: (a) abundant data (2×10^4 trajectories), (b) sparse data (5×10^3 trajectories), (c) 15% measurement noise (2×10^4 trajectories), and (d) 15% dynamic noise (2×10^4 trajectories).

called the deformation gradient tensor, gives

$$\Delta\vec{x}_{n+1} \approx -F\Delta\vec{x}_n. \tag{4}$$

Eq. (4) may be transformed to a coordinate system which diagonalizes F, and only the separation magnitude is of concern:

$$\|\tilde{\Delta\vec{x}}_{n+1}\| = \sqrt{\|\tilde{\Delta\vec{x}}_n F_D^T F_D \tilde{\Delta\vec{x}}_n\|}, \tag{5}$$

where $\tilde{}$ represents vectors in the diagonalized space, the superscripted T represents the transpose, F_D is F diagonalized, and $F_D^T F_D \equiv C_D$ is the right Cauchy Green strain tensor.

Maximum stretching is associated with the invariant manifolds, so only the maximum eigenvalue of C_D ($\lambda_{\max}$) is considered and assuming $\Delta\vec{x}$ is oriented along the direction of the maximum eigenvalue

$$\left\| \frac{\tilde{\Delta\vec{x}}_{n+1}}{\tilde{\Delta\vec{x}}_n} \right\| = \sqrt{\lambda_{\max}}. \tag{6}$$

The FTLE (a measure of stretching in continuous flows) is then defined as

$$\sigma_{t_0}^T \equiv \frac{1}{|T|} \ln\sqrt{\lambda_{\max}}, \tag{7}$$

where T is the evolution time spanned by the map $\vec{\varphi}$. If local stretching is of interest, short T is considered, and the FTLE is averaged along the trajectory to yield an average FTLE. Other variations exist such as the finite-size Lyapunov exponent, which measures the time taken for stretching to reach a certain threshold [22].

We see the above particle divergence schemes can be put into the FTLE formalism, and when the underlying flow field is given many variations exist. The standard technique, with knowledge of the flow, is to iterate a grid of initial conditions and use a simple finite difference scheme to approximate C_D. For irregularly spaced trajectories without flow knowledge, we propose the following: (1) at time zero, locate a cloud of nearest neighbor trajectories to some initial state and (2) then track the cloud for some length of time and quantify its deformation by use of the singular value decomposition (SVD). SVD has the geometric interpretation of an ellipsoid encompassing the cloud, with the singular values (sv) corresponding to the lengths of its semi-axes. The difference between the singular values ($\gamma = sv_1 - sv_2$, where the singular values are ordered by $sv_i \geqq sv_{i+1}$) provides a measure of the clouds elongation. The difference between the final and initial elongation of the cloud ($S = \gamma_f - \gamma_i$) will provide a measure of the stretching experienced by the cloud. Maxima of S will correspond to the locations of maximum stretching and thus approximate the location of the stable manifold as shown in Fig. 4. When considering a system with more than two dimensions, it may be appropriate to use other relationship between the singular values (such as their ratio) to quantify the cloud's elongation. If desired, renormalization may be implemented, and the method may easily be put into the FTLE formalism.

3.3. Velocity field reconstruction

Two of the methods we will consider (FTLE and PSW) make use of reconstructed flow fields, though neither of these methods rely on flow field reconstruction. PSW is a concept and, as will be shown below, this concept may be implemented in different ways, much like FTLE is a measure of stretching, which may be measured in different ways. Indeed, all methods considered would benefit from reconstructed flow fields, but PSW and FTLE are most suited to such structured data. As trajectory data is already available, it may be used to approximate a flow field. There are many ways of converting trajectory data to flow data. The simplest is to consider the displacement vectors over a given time step, however, we have found *local linear models* (LLM) to yield far better results. The flow field is reconstructed as follows:

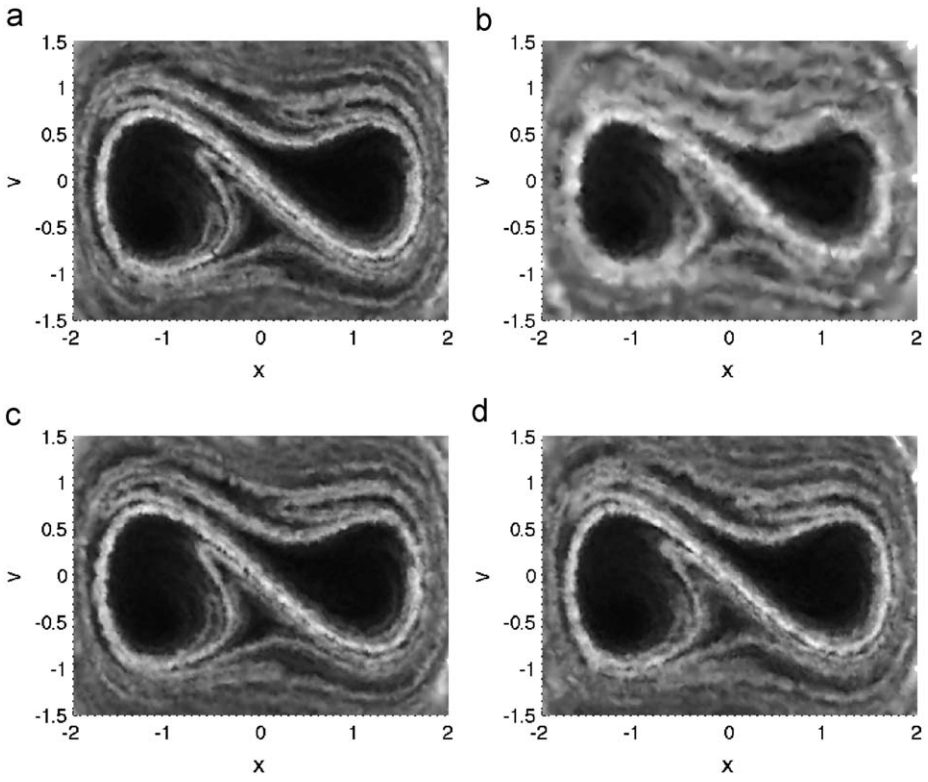

Fig. 4. Manifold approximated by the cloud deformation method: (a) abundant data (2×10^4 trajectories), (b) sparse data (5×10^3 trajectories), (c) 15% measurement noise (2×10^4 trajectories), and (d) 15% dynamic noise (2×10^4 trajectories).

A grid of initial states ($\vec{x}_0$) is chosen. For each initial state a LLM is calculated from N nearest neighbors to that state at that time. The LLM is used to step that trajectory forward one time step. For the next time step, a new LLM is calculated from N nearest neighbors of the new state at the new time and again used to step the trajectory forward in time. This process is repeated for each data set at each initial state for as many time steps as desired. The time step should be chosen small enough that the LLM is applicable, i.e., small enough that the cloud of nearest neighbors does not diverge too much. For our case a time step of $\frac{1}{20}T$ is found to work well. Once the flow field has been reconstructed, we may apply any method, but as this is a time consuming process we only preform reconstruction for those methods which benefit most from it. Note that LLM will only give accurate results for regions of phase space which are suitably populated (enough nearest neighbors close by), and will not yield a complete flow field reconstruction. We are currently considering a dissipative system, so as time evolves, the trajectories are populating a smaller and smaller portion of phase space until all trajectories have converged to the chaotic attractor. However, what the method yields is a good estimate for the evolution of most any trajectory with initial state in the region of phase space populated by stochastic interrogation evolving forward in time.

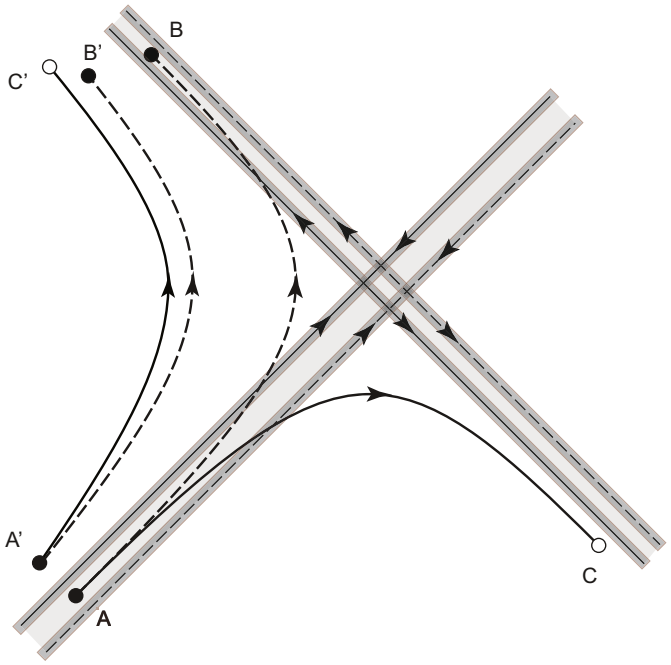

Fig. 6. Example of trajectories evolving from initial states AA′ for a simple saddle (dashed lines) and the same saddle with slightly shifted parameters (solid lines). The evolution from initial states AA′ will depend on which system is used to iterate the trajectory. Points BB′ represent the final states when iterated with the no parameter shifted system, and CC′ represents the final states when iterated with the parameter shifted system. Trajectories which line in the region of manifold shift (light gray area) will be most sensitive to which system they are iterated with. The darker gray region around the manifolds represent the effect of noise (discussed later in Section 4.4).

3.3.1. *Finite-time Lyapunov exponent*

Voth et al. [16] and Haller [17] provide a simple method for calculating the FTLE from flow data. Once a velocity field, $\vec{\psi}$, is given (reconstructed), the deformation gradient tensor $D\vec{\psi}$ can be used to calculate the right Cauchy Green strain tensor, $C_D = (D\vec{\psi})^T(D\vec{\psi})$, where $D\vec{\psi}$ represents the Jacobian. Then Eq. (7) may be used to calculate the FTLE. In our case $\vec{\psi}$ will be the four period map (constructed from a sequence of LLM). This map is then used to calculate a FTLE field. Ridges of this field will approximate the stable manifold's location as shown in Fig. 5. This

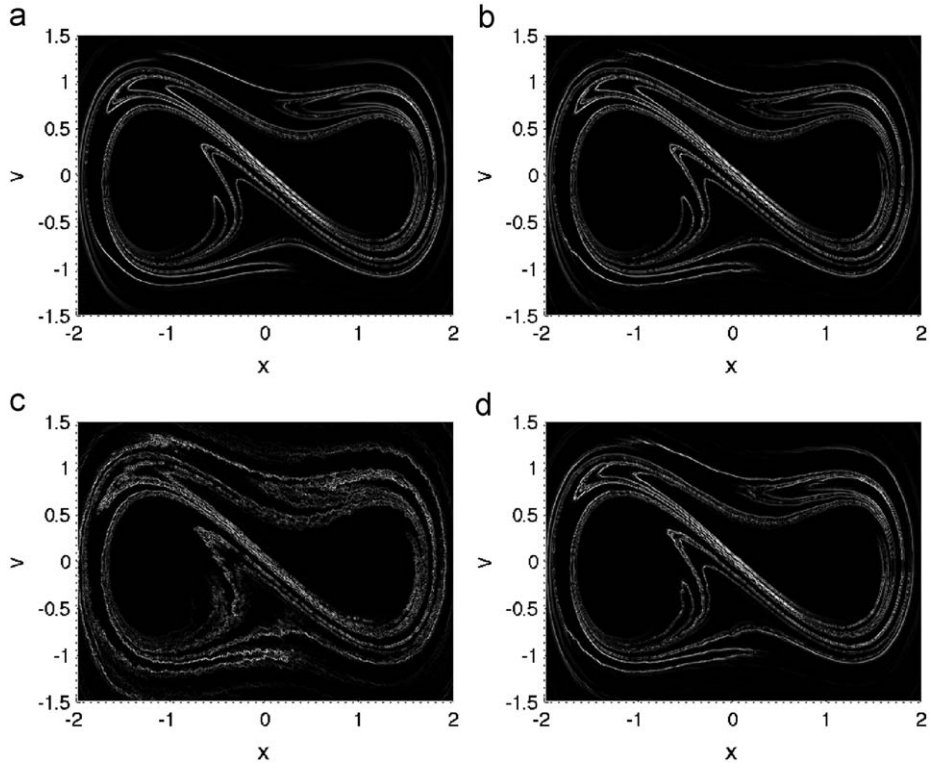

Fig. 5. Manifold approximated from reconstructed velocity field data with a FTLE method: (a) abundant data (2×10^4 trajectories), (b) sparse data (5×10^3 trajectories), (c) 15% measurement noise (2×10^4 trajectories), and (d) 15% dynamic noise (2×10^4 trajectories).

method is sometimes referred to as the direction finite-time Lyapunov exponent or DFTLE, where FTLE then implies renormalization. We will continue to refer to the method as FTLE.

3.3.2. Phase space warping

The new method of manifold identification is based on the concept of *phase space warping* (PSW) [12]. PSW refers to the slight

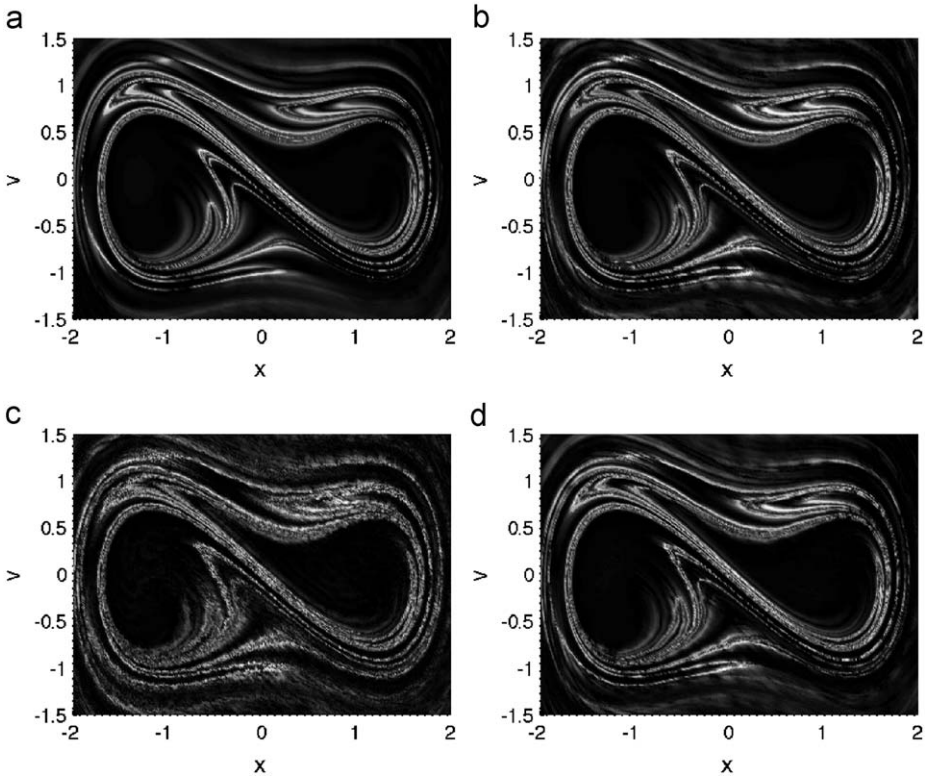

Fig. 7. Manifold approximated by the PSW method, from two LLMs calculated on a 0.01×0.01 mesh grid: (a) abundant data (2×10^4 trajectories), (b) sparse data (5×10^3 trajectories), (c) 15% measurement noise (2×10^4 trajectories), and (d) 15% dynamic noise (2×10^4 trajectories).

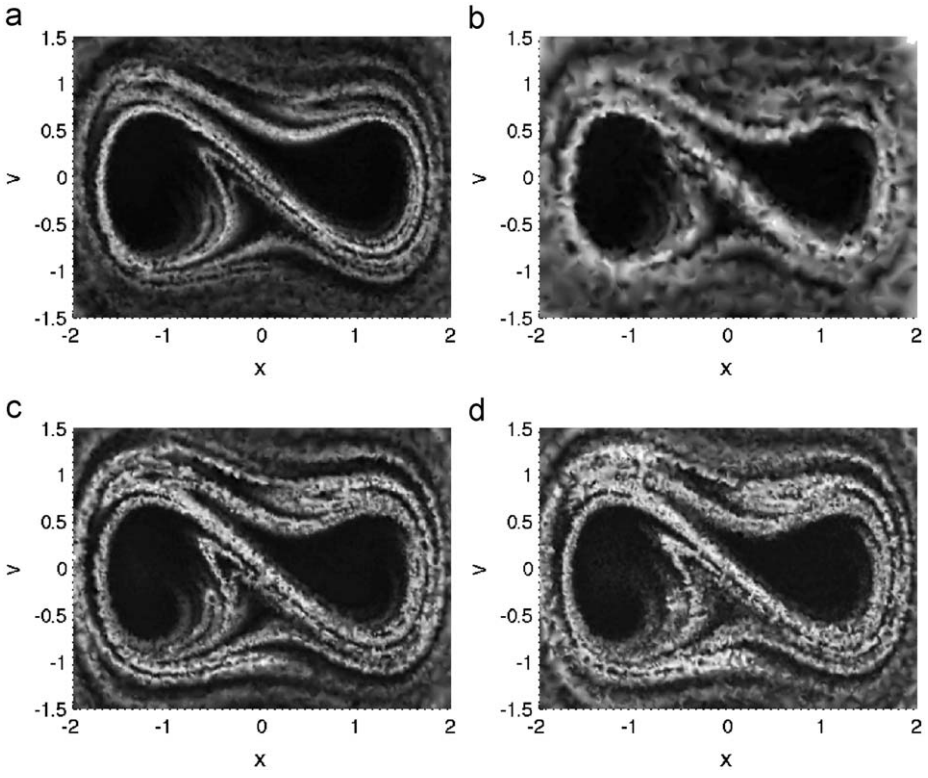

Fig. 8. Manifold approximated by the particle divergence method modified with the PSW concept by addition of a $50^{-1}T$ phase delay: (a) abundant data (2×10^4 trajectories), (b) sparse data (5×10^3 trajectories), (c) 15% measurement noise (2×10^4 trajectories), and (d) 15% dynamic noise (2×10^4 trajectories).

deformation a phase space (or physical space) is subject to under small parameter shifts. This concept is currently being used to track damage/fatigue in mechanical and biological systems [12,18–20]. The "warping" of the phase space may also be taken advantage of to identify the system's invariant manifolds.

Application of the PSW concept is motivated by its geometric interpretation. Consider a simple saddle point (Fig. 6). A slight shift in the parameters of the system cause the geometric structure of the phase space to shift ("warp"). Notice the location of the manifolds for the parameter shifted (solid) and non-shifted (dashed) systems are different. The evolution from initial states located in this region of shift are greatly influenced by which system (parameter shifted or not) is used to iterate them. The shift has caused the initial state to switch sides of the manifold, i.e. basin of attraction, if present. The manifold can then be identified by those trajectories which are most influenced by small shifts in the parameters of the system.

A closer look shows PSW to generalize the FTLE method along with its stretching based interpretation, to a sensitivity based interpretation. While stretching can be thought of as spatial initial condition sensitivity, PSW encompasses sensitivity to all initial conditions (position, time, etc.) and parameters of the system. To illustrate this, consider the map $\vec{\varphi}_T(\vec{x}_0(t_0), \{\alpha\}, t_0)$, where $\{\alpha\}$ represents system parameters (mass, stiffness,...) and $\vec{x}_0$ is the state at time t_0, which maps trajectories T time units forward. If T is the period of a periodic system, then $\vec{\varphi}_T$ is the stroboscopic Poincaré map. PSW considers the differences in trajectories iterated with parameter shifted or unshifted systems.

$$\vec{\Delta}_T^{\alpha} = \vec{\varphi}_T(\vec{x}_0(t_0), \{\alpha+\Delta\alpha\}, t_0) - \vec{\varphi}_T(\vec{x}_0(t_0), \{\alpha\}, t_0), \tag{8}$$

or

$$\vec{\Delta}_T^{t} = \vec{\varphi}_T(\vec{x}_0(t_0), \{\alpha\}, t_0+\Delta t) - \vec{\varphi}_T(\vec{x}_0(t_0), \{\alpha\}, t_0), \tag{9}$$

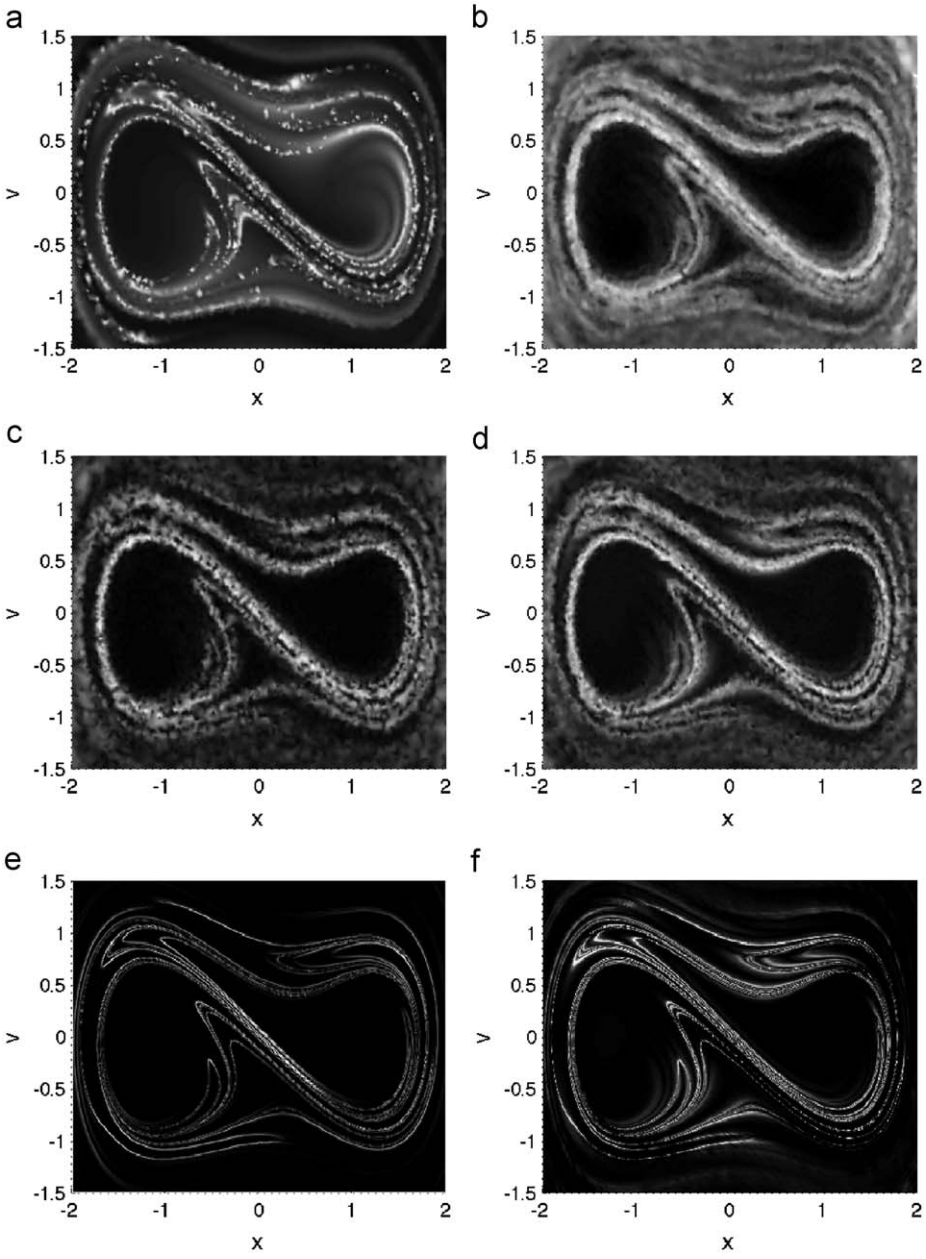

Fig. 9. Comparison figure of each method for abundant data (2×10^4 trajectories) with no noise: (a) closest approach, (b) cloud deformation, (c) particle divergence, (d) particle divergence with PSW, (e) FTLE applied to reconstructed flow data, and (f) PSW.

where $\Delta\alpha$ and Δt represent small shifts of a system parameter or time, respectively. In either case, Taylor expansion about the small perturbation yields, to the first order,

$$\delta_\alpha \equiv \frac{\|\vec{\Delta}_T^{\alpha}\|}{\|\Delta\alpha\|} \approx \left\| \frac{d\vec{\varphi}_T(\vec{x}_0(t_0), \{\alpha\}, t_0)}{d\alpha} \right\|, \tag{10}$$

or

$$\delta_t \equiv \frac{\|\vec{\Delta}_T^{t}\|}{\|\Delta t\|} \approx \left\| \frac{d\vec{\varphi}_T(\vec{x}_0(t_0), \{\alpha\}, t_0)}{dt} \right\|. \tag{11}$$

These are the rate of change of the $\vec{\varphi}_T$ with respect to the shifted parameters. Note that even though $\vec{\varphi}_T$ represents an integrated trajectory, this is the "Eulerian" time derivative, *not* the "Lagrangian" time derivative. There is no parametric dependence on time. This is because we are holding the initial position, $\vec{x}_0$, fixed, and evaluating the rate of change at a fixed location. With the geometric interpretation in mind, we see that those trajectories which maximize δ will approximate the stable manifold.

The realization of this method for trajectory data requires two data sets with slightly different parameters. Time (or phase for periodically forced systems) is a convenient parameter to investigate. The second data set is thus constructed by slightly time delaying the first data set (say one sampling interval). After successive LLM applications, the result will be a set of trajectories for data set 1 ($\vec{\chi}_1(t;\vec{x}_0,t_0)$) and data set 2 ($\vec{\chi}_2(t;\vec{x}_0,t_0)$). The difference/error $(\vec{\Delta}_T^{t}(t;\vec{x}_0,t_0) = \vec{\chi}_2(t;\vec{x}_0,t_0) - \vec{\chi}_1(t;\vec{x}_0,t_0))$ between the two sets of trajectories is calculated. The small time shift has allowed the location of the manifolds to evolve slightly. δ_t will be largest for those initial states which lie in the region where the

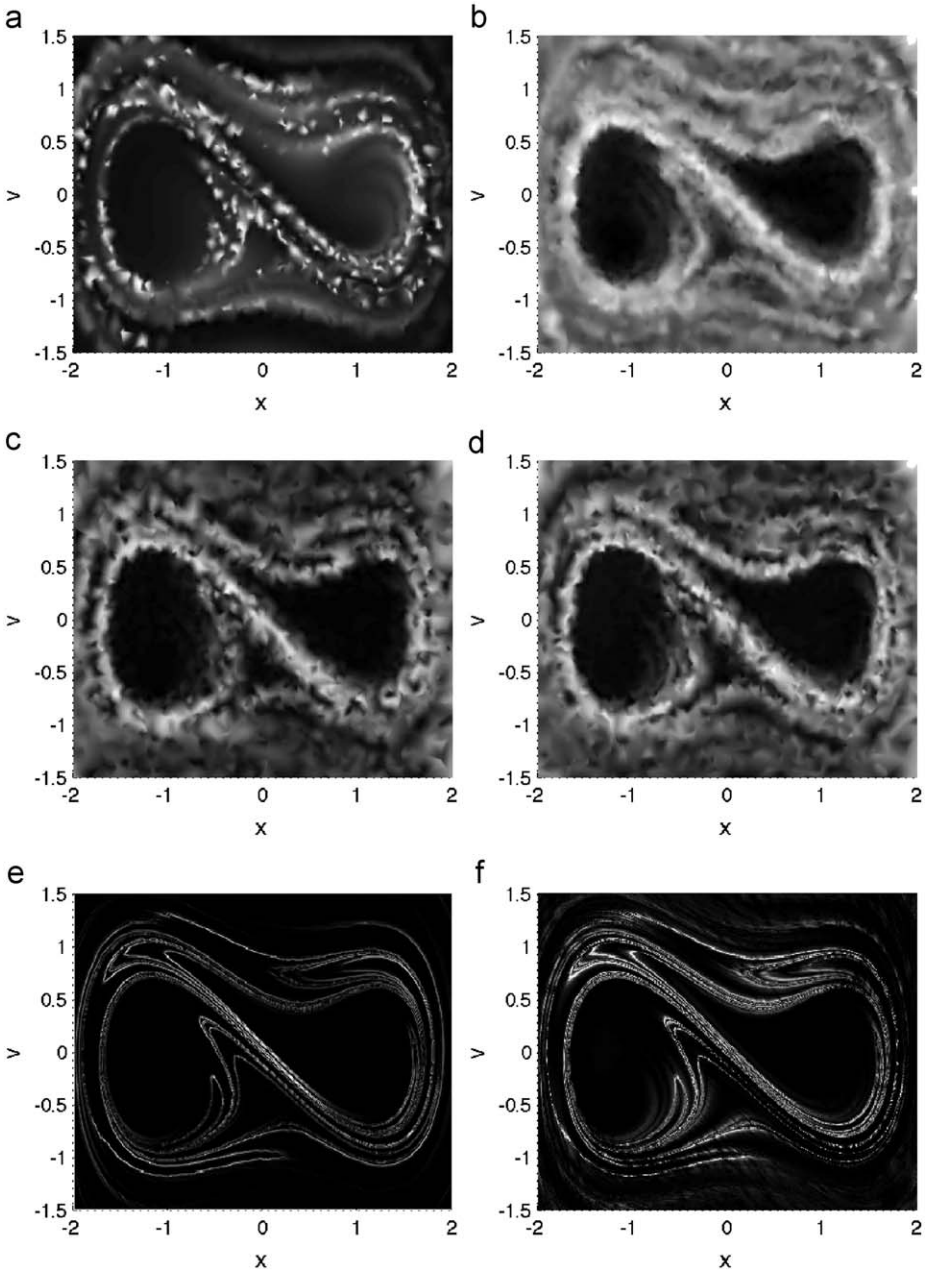

Fig. 10. Comparison figure of each method for sparse data (5×10^3 trajectories) with no noise: (a) closest approach, (b) cloud deformation, (c) particle divergence, (d) particle divergence with PSW, (e) FTLE applied to reconstructed flow data, and (f) PSW.

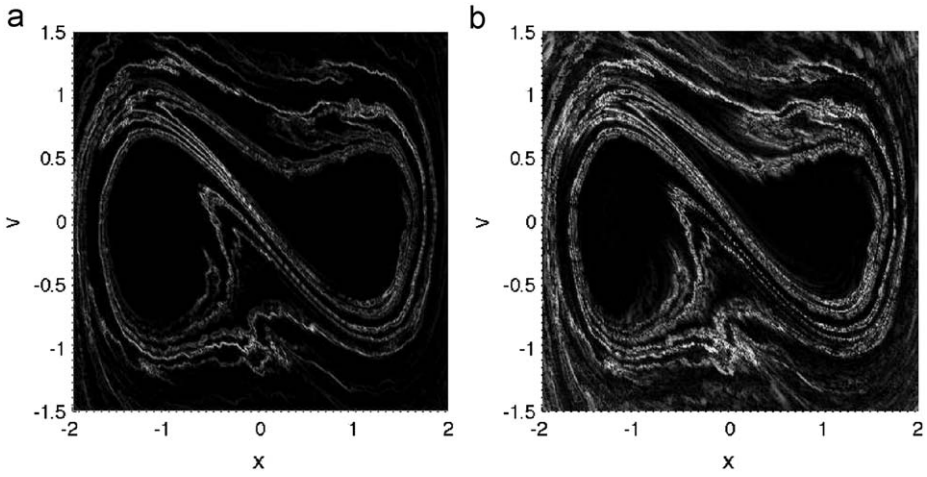

Fig. 11. Comparison figure for severely limited data (1×10^3 trajectories) with no noise: (a) FTLE and (b) PSW.

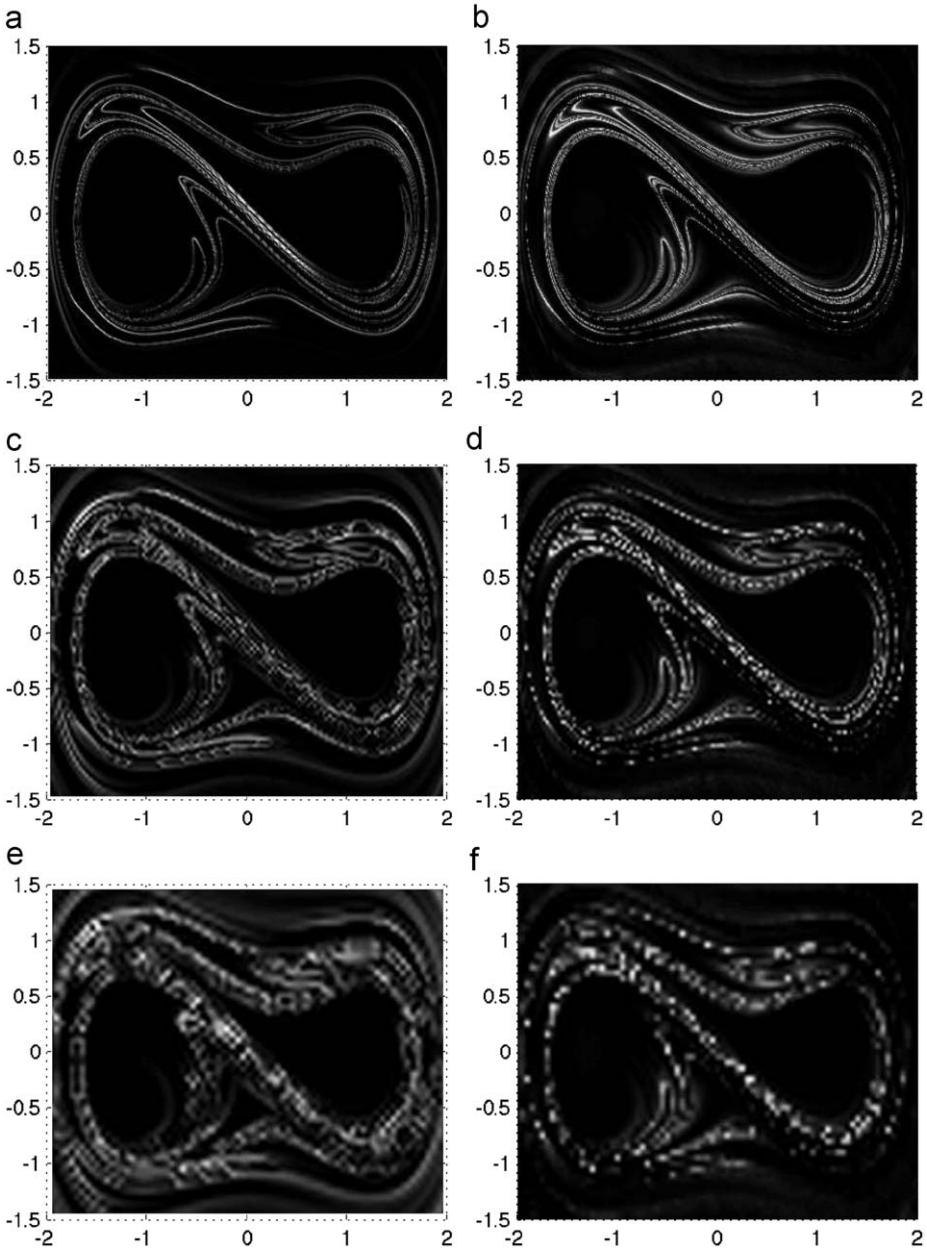

Fig. 12. Comparison between FTLE and PSW for different initial position grid spacings used to calculate LLM ($dx = 0.01$): (a) FTLE, (b) PSW ($dx = 0.03$), (c) FTLE, (d) PSW ($dx = 0.05$), (e) FTLE, and (f) PSW.

manifolds have shifted. Since the region is small, due to the small time shift, the ridges of δ_t will approximate the location of the invariant manifolds (see Fig. 7). The magnitude of the time shift will be dependent on the system under consideration, though an advective time scale based on the characteristic phase space "velocity" and average initial state separation would provide an estimated lower limit.

Experimentally, time is not the only parameter which may be considered. Any parameter which causes the manifolds to shift will do. This may be accomplished by addition of a small mass or spring, or by allowing the system to fatigue. Note that the magnitude of manifold shift will be related to the magnitude of the parameter shift. If this shift is too large, the manifolds will also shift too much, and their positions cannot be identified accurately. However, if the parameter shift is too small, the manifold shift will be too small for the grid of initial conditions to locate.

The PSW concept may also be applied to other methods to improve their detection. We modify the particle divergence method by adding a $50^{-1}T$ phase delay when calculating the nearest neighbors (which are otherwise calculated at the same time). Fig. 8 shows this to be an improvement over the non-shifted data set. Note that this is a way to implement PSW without reconstructing the flow field.

4. Discussion

4.1. Ideal case—noise-free abundant data

When data is abundant (2×10^5 trajectories) and noise is absent each method is capable of identifying the invariant manifolds of the system (Fig. 9 compared with Fig. 1). PSW and FTLE computed from reconstructed flow data seem to be the most

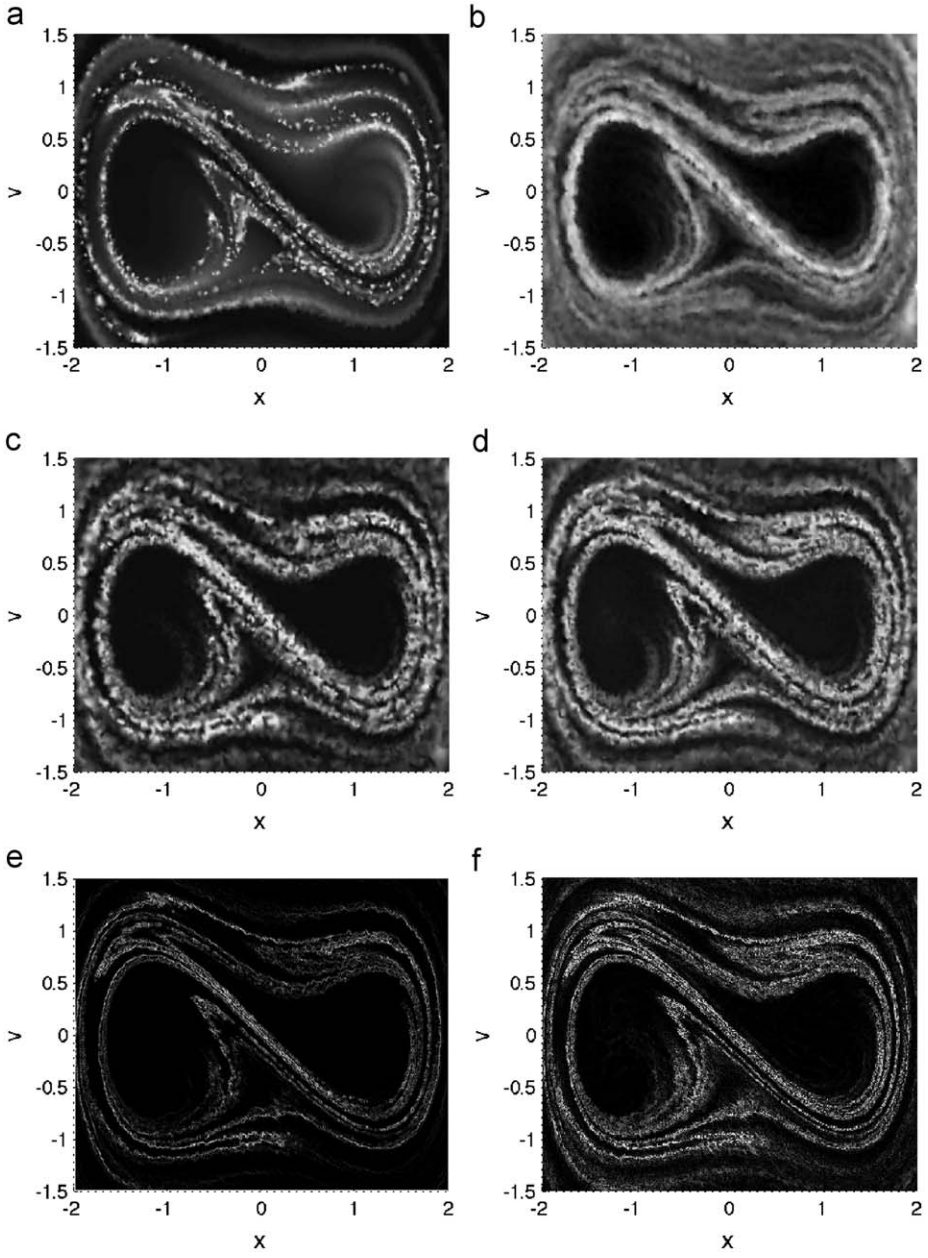

Fig. 13. Comparison figure for abundant data (2×10^4 trajectories) at the 15% measurement noise level: (a) closest approach, (b) cloud deformation, (c) particle divergence, (d) particle divergence with PSW, (e) FTLE applied to reconstructed flow data, and (f) PSW.

successful. This is in part due to the interpolation (LLM) present in those methods, though without the interpolation FTLE and PSW continue to out preform the other methods but to a lower degree. The closest approach method, particle divergence methods, and cloud deformation method have no interpolation, and can be relied upon to represent only what the raw data permits. The resulting images are spiky and noisy as a result of the randomly populated phase space, though these effects diminish as data abundance increases. PSW and velocity field reconstruction images contain smoother, better defined ridges, which resemble manifolds calculated with knowledge of the flow field. FTLE identifies sharp peaks which identify the manifolds position, while PSW identifies the region of manifold shift, which gives the effective manifold location (or effective basins of attraction) subject so some parameter tolerances. In applications where system parameters are only know within some range (stiffness, mass, ..., tolerances), this may be a more useful quantity than exact manifold locations.

4.2. Limited data case

As data becomes limited, the success of all methods is reduced (Fig. 10). However, PSW and FTLE identification are least affected. This has little to do with the individual methods, but is a result the LLM ability to reproduce the flow. Even for severely limited data (1000 trajectories, Fig. 11), the flow field is reasonably reconstructed and manifold structure is apparent. This shows that the LLM reconstruction performs well for small amount of data, which is particularly important for higher dimensional systems. However, the limiting factor then becomes computation time required to compute the LLM. In this case, a better measure

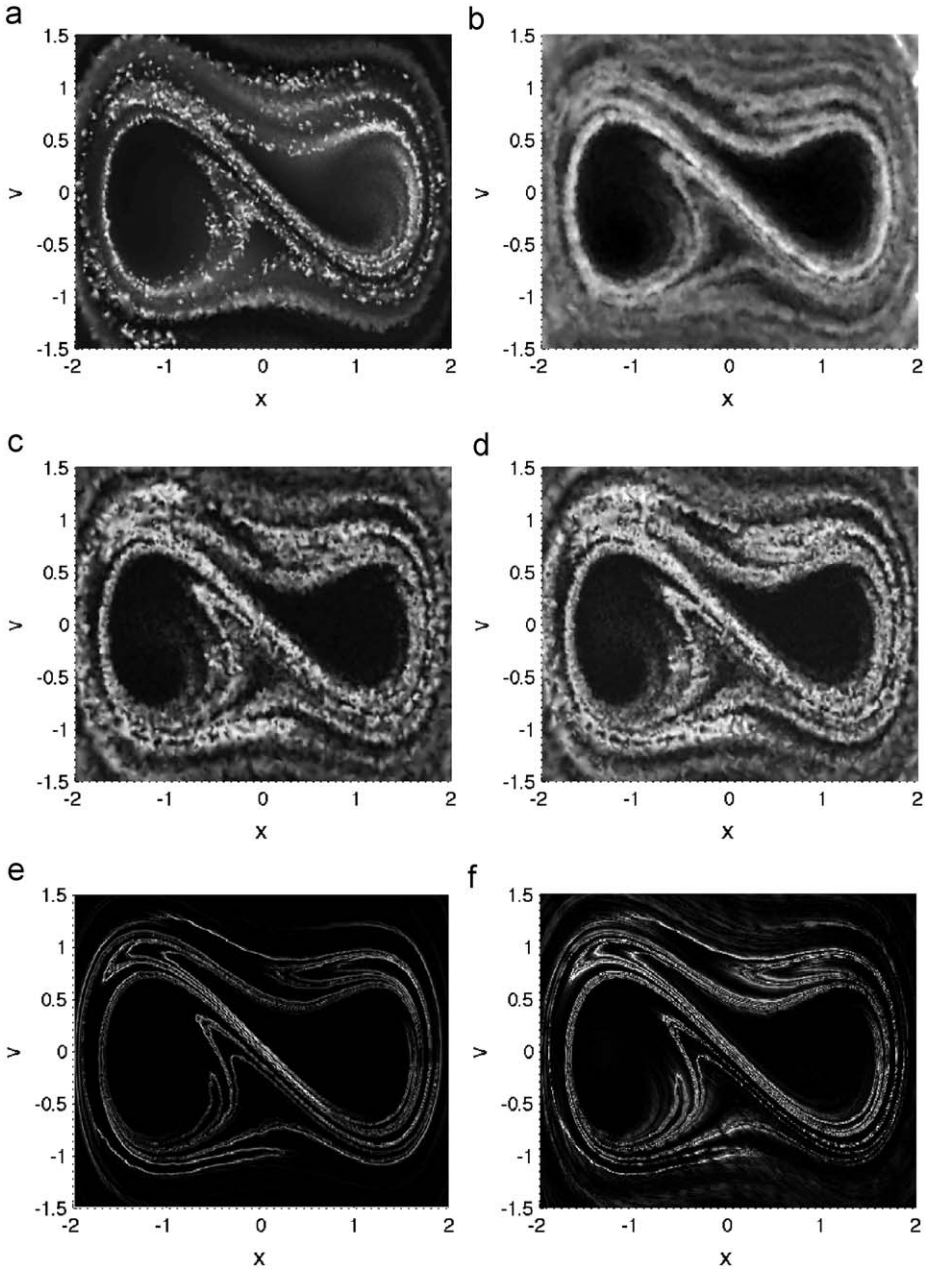

Fig. 14. Comparison figure for abundant data (2×10^4 trajectories) at the 15% dynamic noise level: (a) closest approach, (b) cloud deformation, (c) particle divergence, (d) particle divergence with PSW, (e) FTLE applied to reconstructed flow data, and (f) PSW.

of limited data is how coarse the grid of initial states used for LLM calculations is. As we vary this grid resolutions, we see PSW out preforms FTLE as grid spacing is increased (Fig. 12). The reason for the success of PSW is that it tends to only identify the region of manifold shift. As long as there is sufficient data to populate this region, PSW will identify it. Therefore, when data is severely limited it may be necessary to increase the parameter shift between data sets. This will increase the region of manifold shift, making the region more likely to be populated at the expense of broader ridges. On the other hand, FTLE will always identify manifolds, but with a detection accuracy that depends directly on Δx.

4.3. Additive measurement noise case

Measurement noise is additive and represents an uncertainty in the measured state of the system. The effects of this type of noise on each detection scheme are not unexpected. It results in a broadening/blurring of the peaks and a reduction of the fine, long-time structures. At the 15% level, the performance of all methods is significantly reduced (Fig. 13), however, when considering the relative degradation of each method against its noise free performance, the particle divergence and particularly the cloud deformation schemes appear to be the least sensitive to measurement noise.

4.4. Dynamics noise case

Dynamic noise was incorporated into the system by addition of a random number to the amplitude of the forcing term. A geometric interpretation of dynamic noise is to consider the noise free manifolds wiggling in time. A definition for invariant manifolds in this situation is even more unclear than for the standard finite-time aperiodic case. However, from an experimental point-of-view, noise is always present and must be accounted for. Regardless of a clear definition, we are interested in manifold like behavior, and seek to identify structures in the flow which exhibit such behavior. At the 15% dynamic noise level, all methods show indications of manifold like behavior (Fig. 14). Though, only FTLE and PSW methods provide clear structures.

5. Conclusion

The lack of knowledge of a flow field or equations of motion, is not a barrier to invariant manifold detection, if trajectory data is provided. We have shown that simple adaptations of existing manifold detections schemes are capable of identifying invariant manifold like behavior of a system, and explored the new PSW method as a means to identify invariant manifolds for trajectory only data. The results of our investigation show that when detecting invariant manifold like behavior in experimental data: fast and simple first attempt methods such as the approach and pair divergence methods may be used for rough manifold location, though these are severally effected by noise and data limitations. If measurement noise is expected to be large the cloud deformation method with a large amount of data provides best results. However, in general, use LLM to reconstruct flow, and apply FTLE to get accurate manifold location or PSW to get effective manifold location subject to some parameter range. When computation time is a factor, reduce the grid resolution of initial positions used for LLM calculation and apply PSW for best results. This is likely to be important when considering higher dimensional problems. We have shown LLM reproduce the flow structure well for very limited data, though this will depend on the system being considered. Thus, in higher dimensional problems computation time, rather than data collection time, is likely to be the main obstacle. Our results suggest PSW is likely to be useful in these situations. However, general stretching bases methods (FTLE, cloud deformation, pair divergence) should always identify manifold like behavior, but with less resolution as data become sparse. PSW, on the other hand, will only identify the region of manifold shift. If this region is not populated, PSW will not identify it.

This suggests an interesting application of the PSW method in control scheme implementation. Assume a system has several basins of attraction and one of those basins possess some desirable properties. Thus, we want to impose control to remain in or reenter the desirable basin. The optimal location to apply such a control is where basin boundaries are most or least robust. This is precisely what PSW identifies. PSW identifies narrow ridges in those locations where the manifolds are least sensitive to system tolerances, optimal reentrance locations, and wide ridges in those locations where manifolds are highly sensitive to system tolerances, locations most likely to eject trajectories from the basin.

The demonstrated success of the PSW method for limited data and its generalization of the popular FTLE method warrants a more rigorous treatment. It is our hope that this method may provide new insight and understanding for manifold like behavior in finite-time aperiodic flows. Thus, ongoing research is focused on the implication of the PSW interpretation of invariant manifolds, along with modifications to the basic concept introduced here. We also hope to apply PSW to a variety of actual experimental data sets to further test its applicability and explore higher dimensional problems.

Acknowledgments

The authors would like to thank the anonymous reviews for insightful comments and constructive criticism which greatly improved this manuscript. This paper is based on work supported by NSF Grant no. CMS-0237792.

References

[1] P.D. Miller, L.J. Pratt, K.R. Helfrich, C.K.T.T. Jones, Chaotic transport of mass and potential vorticity for an island recirculation, Journal of Physical Oceanography 32 (2002) 80–101.
[2] R.C. Hilborn, Chaos and Nonlinear Dynamics, Oxford University Press, Oxford, 2000.
[3] A.M. Mancho, D. Small, S. Wiggins, A tutorial on dynamical systems concepts applied to lagrangian transport in oceanic flows defined as finite time data sets: theoretical and computational issues, Physics Reports 437 (2006) 55–124.
[4] M. Mathur, G. Haller, T. Peacock, J.E. Ruppert-Felsot, H.L. Swinney, Uncovering the lagrangian skeleton of turbulence, Physical Review Letters 98 (2007) 1445021–1445024.
[5] S. Wiggins, The dynamical systems approach to lagrangian transport in oceanic flows, Annual Review of Fluid Mechanics 37 (2005) 295–328.
[6] K. Ide, D. Small, S. Wiggins, Distinguished hyperbolic trajectories in time-dependent fluid flows: analytical and computational approach for velocity fields defined as data sets, Nonlinear Processes in Geophysics 9 (2002) 237–263.
[7] S.C. Shadden, F. Lekien, J.E. Marsden, Definition and properties of lagrangian coherent structures from finite-time Lyapunov exponents in two-dimensional aperiodic flows, Physica D 212 (2005) 271–304.
[8] F.C. Moon, P. Holms, A magnetoelastic strange attractor, Journal of Sound and Vibration 65 (2) (1979) 275–296.
[9] J.P. Cusumano, B.W. Kimble, A stochastic interrogation method for experimental measurements of global dynamics and basin evolution: application to a two-well oscillator, Nonlinear Dynamics 8 (1995) 213–235.
[10] B.W. Kimble, J.P. Cusumano, Theoretical and numerical validation of the stochastic interrogation experimental method, Journal of Vibration and Control 2 (1996) 323–348.
[11] K.P. Bowman, L.L. Pan, T. Campos, R. Gao, Observations of fine-scale transport structure in the upper troposphere from the high-performance instrumented airborne platform for environmental research, Journal of Geophysical Research 112 (2007) 1–10.
[12] D. Chelidze, J.P. Cusumano, Phase space warping: nonlinear time series analysis for slowly drifting systems, Philosophical Transactions of the Royal Society A 364 (2006) 2495–2513.

[13] A.M. Mancho, D. Small, S. Wiggins, K. Ide, Computation of stable and unstable manifolds of hyperbolic trajectories in two-dimensional, aperiodically time-dependent vector fields, Physica D 182 (2003) 188–222.
[14] S. Winkler, Lagrangian dynamics in geophysical fluid flows, Ph.D. Thesis, Division of Applied Mathematics, Brown University, May 2001.
[15] A. Wolf, J. Swift, H. Swinney, J. Vastano, Determining Lyapunov exponents from a time-series, Physica D 16 (1985) 285–317.
[16] G.A. Voth, G. Haller, J. Gollub, Experimental measurements of stretching fields in fluid mixing, Physical Review Letters 88 (25) (2002) 25.
[17] G. Haller, Distinguished material surfaces and coherent structures in three-dimensional fluid flows, Physica D 149 (2001) 248–277.
[18] D. Chelidze, M. Liu, Reconstructing slow-time dynamics from fast-time measurements, Philosophical Transactions of the Royal Society A 336 (2008) 729–745.
[19] J. Dingwell, D. Napolitano, D. Chelidze, A nonlinear approach to tracking slow-time-scale changes in movement kinematics, Journal of Biomechanics 40 (2006) 1629–1634.
[20] M. Song, D.B. Segala, D. Chelidze, J.B. Dingwell, Slow-time changes in human muscle fatigue are fully represented in movement kinematics, Journal of Biomechanical Engineering 131 (2009) 021004.
[21] J.C. Sprott, Chaos and Time-Series Analysis, Oxford University Press, Oxford, 2003.
[22] A. Aurell, G. Boffetta, A. Crisanti, G. Paladin, A. Vulpiani, Predictability in the large: an extension of the concept of Lyapunov exponent, Journal of Physics A: Mathematical and General 30 (1997) 1–26.
[23] J.A.J. Madrid, A.M. Mancho, 2009. Distinguished trajectories in time dependent vector fields. Chaos 19, 013111-1–013111-18.
[24] G. Haller, Finding finite-time invariant manifolds in two-dimensional velocity fields, Chaos 10 (1) (2000) 99–108.